Material Characterization on the Affected Zones by Fine Piercing into Single Crystal Fe-6Si Steel Sheet

WCMNM 2021

Tatsuhiko Aizawa[1] Tomomi Shiratori[2] Tomoaki Yoshino[3] Kunaiki Dohda[4]

[1]*Surface Engineering Design Laboratory, SIT, Japan*
[2] *University of Toyama, Japan*
[3] *Komatsu-Seiki Kosakusho, Co., Ltd., Japan*
[4]*Nothwestern University, USA*

Abstract

Magnetism in motor core was often reduced by formation of plastically affected zones by work material flow in piercing the electrical steel sheets. This iron loss was minimized by improving the preciseness in piercing. A platform methodology to make quantitative evaluation on these affected zones in the pierced electrical steel sheets was proposed to search for the way to minimize the iron loss. Coarse-grained electrical steel sheet was employed for fine piercing experiment under the narrowed clearance between the plasma nitrided punch and core-die. The shearing behavior by the applied loading for piercing was described by in situ measurement of load-stroke relationship. The plastic straining in the single-crystal electrical steel sheet was characterized by SEM and EBSD to define the affected zones size and analyze the rotation of crystallographic orientations by the induced plastic distortion during piercing.

Keywords: Motor core, Electrical steel sheet, single crystal, plastically affected zone by piercing, plastic straining, spinning, EBSD, crystallographic characterization

1. Introduction

A motor core is one of the most essential parts not only in electric vehicles but also in passenger and commodity cars [1]. In addition to a large-scaled driving unit, small and tiny motors work in these automobiles to improve the comfortable driving conditions. Hence, the energy loss in working those motors must be reduced as possible to lower CO_2 emission during driving [2]. As surveyed in [3], the energy inefficiency comes from various losses generated in shaping the electrical steel sheets. In particular, the plastically affected zones left in the steel sheets by piercing is responsible for hysteresis loss [4]. Reduction of this affected zone size, becomes an engineering issue in fabrication of high quality motor cores [5]. Authors proposed a way to aim at high-quality piercing by sharpening the punch edge [6], by using the nitrided punch and die under nearly zero clearance [7-8], and by laser-trimming the diamond coated WC (Co) punch [9-10]. How to characterize the mechanical interaction between electrical steel sheets and piercing punch, grows to be a problem to guide the research for reduction of the affected zone size by fine piercing.

In the present study, a new approach is proposed to describe the fine piercing process by using a single crystal Fe-6Si steel sheets. Since single crystals are aligned in the work material sheet, the piercing process is performed as a perforation process into a selected single crystal with the specified crystallographic orientation by indentation of punch under the narrowed and nearly zero clearance. SEM (Scanning Electron Microscopy) – EDX (Electron Diffraction X-Ray Spectroscopy) as well as EBSD (Electron Back-Scattering Diffraction) are utilized to describe the shearing process when piercing with the use of plasma-nitrided punch and core-die. The pierced single-crystal specimen is prepared for EBSD analysis [11] with aid of the elasto-plastic analysis [12] to describe the plastic straining and spin-rotation in fine piercing. The plastically affected and plastic zones are defined to have significant spin rotations and plastic strains, respectively.

2. Experimental Procedure

2.1. Characterization on the straining and spinning

A single crystal of electrical steel sheet is employed to characterize the piercing process. With the slip-line theory [13], a platform of shearing test is constructed, as illustrated in Figure 1, to quantitatively describe the strained zones left in the pierced crystal. When piercing the selected single crystal under the nearly zero clearance, the residual distortion is minimized around the vicinity of perforated hole with the radius of r_0. After EBSD, the region with $r_0 < r < r_1$, is characterized as a grain-size refined area with large spinning (ω) to be analyzed by IPF (inverse pole figure). This first zone is surrounded by the region with $r_1 < r < r_2$.

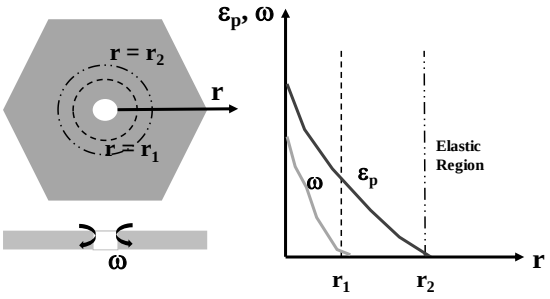

Figure 1. Platform to characterize the piercing process into a single crystal of electromagnetic sheet.

This boundary at $r = r_2$ is estimated by KAM (Kernel Angle Misorientation) mapping in EBSD and by slip-line field theory for the indentation of rigid punch to the rigid-plastic work-material [13]. These two

regions are elastically constrained in the original single crystal. The first region with large spin rotation is identified as a crystallographically affected zone of electrical steel sheets. The second region with residual plastic strains is recognized as a mechanically affected zone. In the following EBSD measurement, the top and cross-sectional surfaces of selected single crystals are analyzed to estimate both IPF and KAM distributions.

2.2. Nitrided punch and die

A pair of SKD11 punch and core-die was prepared and plasma nitrided at 673 K for 14.4 ks by 70 Pa. Figure 2 shows the nitrided punch and die for fine piercing experiment. The measured clearance between these punch and die is 1.5 % of the sheet thickness.

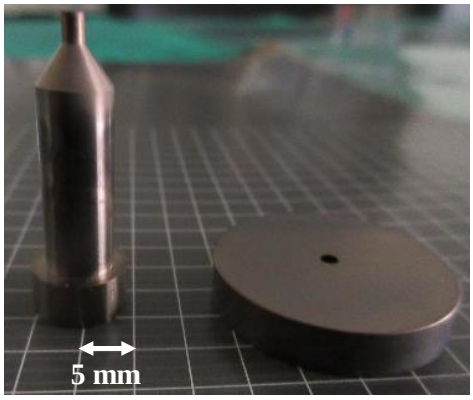

Figure 2. Plasma nitrided SKD11 punch and die with the hardness of 1400 HV and the nitrided layer thickness of 40 μm.

2.3. CNC-stamper for fine piercing

These punch and core-die is fixed into a cassette die set and cemented to upper and lower bolsters of CNC (Computer Numerical Control)-stamping system, as shown in Figure 3. A load-cell is embedded into the lower die to monitor the applied load.

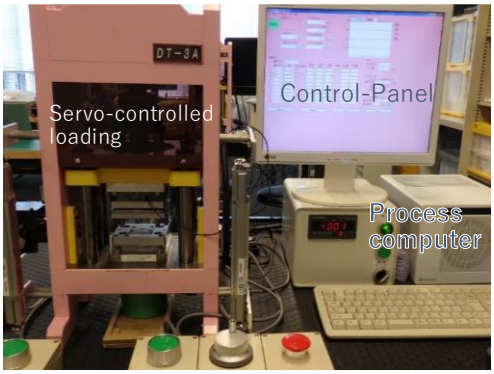

Figure 3. CNC-stamping system for fine piercing under nearly zero-clearance between punch and die.

2.4. Work materials

Grain oriented electrical steel sheet was prepared by rolling and annealing processes as illustrated in Figure 4a). This coarse-grained sheet specimen has larger grains than 10 mm and smaller grains than 5 mm. Former grain orientations are often aligned along the axis of easy magnetization <001> by rolling and annealing. While, latter grains have misorientations to this axis so that the effect of original crystallographic orientation on the affected zone formation by piercing is described by selecting these smaller grains. Since the sheet thickness is only 0.2 mm, each grain has homogeneous microstructure in thickness In Figure 4b.

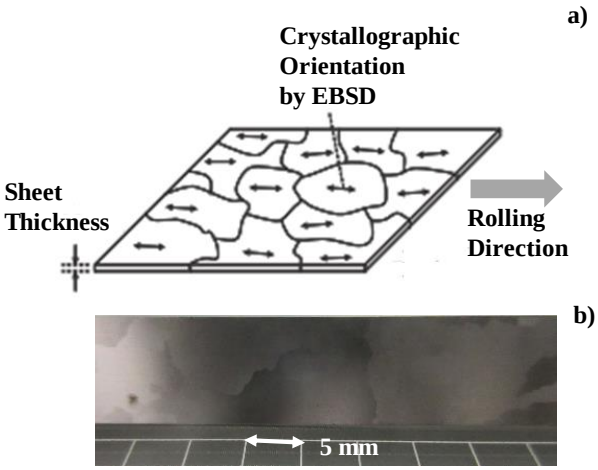

Figure 4. Coarse-grained electrical sheet by rolling. a) Schematic view of coarse-grained sheet, and b) work specimen for the present fine piercing experiment.

3. Experimental Results and Discussion

3.1. Piercing process

A pair of nitrided SKD11 punch and die was utilized for piercing process. Among several coarse grains in the specimen, three grains with the average size of 8 mm were selected as a work material in the following experiments, in Figure 4b).

Figure 5 shows the pierced single Fe-6Si crystals by piercing experiments. Among several testpieces, the pierced crystal with No. 1 was selected for the following material characterization.

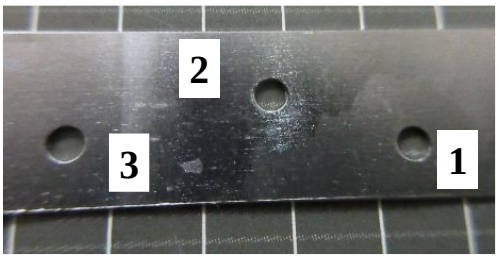

Figure 5. Pierced holes in the designated crystal in the coarse-grained sheet.

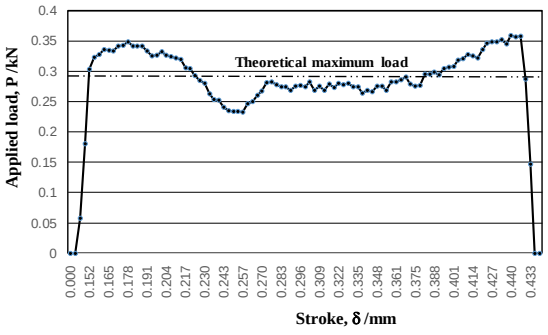

Figure 6. Applied load – stroke relationship during the piercing process.

The applied load was monitored by the load cell for each stroke. Figure 6 depicts the applied load – stroke relationship. Assuming that the piercing advances in simple shear stress, the maximum load (P_{max}) is estimated to be $P_{max} = \pi D \times \kappa \times t$, where D is the punch diameter, κ, the shear yield stress and t, the sheet thickness. Since D = 2 mm, $k = \sigma_y / \sqrt{3}$ MPa for σ_y, the uniaxial yield stress = 400 MPa, and t = 0.2 mm, P_{max} = 0.29 kN.

3.2. EBSD analysis of pierced single crystal

The specimen for material characterization by SEM-EDX and EBSD was prepared after cutting and polishing. Figure 7 depicts the test-piece of single crystal #1, cut from the original specimen in Fig. 5. The pierced hole was embedded by the lead-free solder to prevent from distortion during cutting and polishing. The analysis region was selected at the zone with the least scratches by polishing.

Figure 7 depicts the SEM and YAG-BSE (YAG-detected back-scattered electron) images on the top surface at the vicinity of the pierced hole in low and high magnifications, respectively. Besides for the mechanical scratches by polishing, these images are classified into three regions; e.g., the region-1 just around the pierced hole, and the region-2 with different contrast from the surrounding region-3.

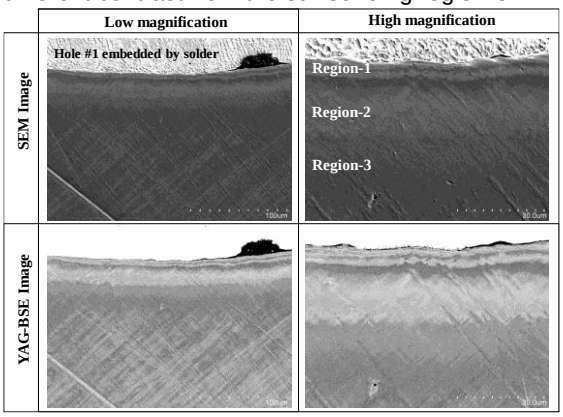

Figure 7 SEM and YAG-BSE images on the polished surface at the vicinity of the pierced hole in the low and high magnifications.

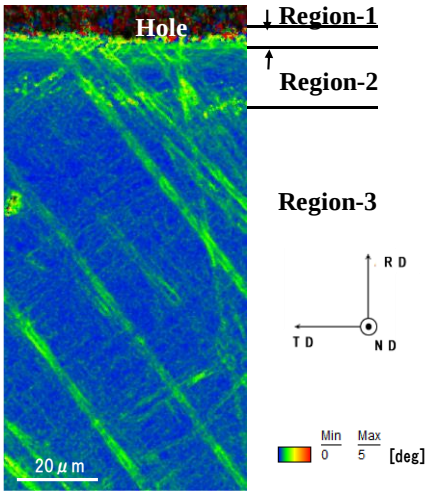

Figure 8. KAM distribution in ND (Normal direction) or along the top surface of pierced single crystal.

After [11, 14], the KAM distribution describes the equivalent plastic strain distribution. The KAM regions with higher misorientation angle corresponds to elasto-plastic region. Figure 8 shows the KAM distribution in the ND direction on the top view of pierced single crystal. Besides for noises by residual polished traces, the whole surface is classified into three regions in correspondence to SEM and YAG-BSE images in Fig. 7. In the region-1 with 0 < r < 5 μm, the misorientation angle is uniformly high; microstructure changes by the piercing process together with plastic strain localization [13]. In the region-2 with 5 μm < r < 20 μm, high angled KAM distributes sparsely on the surface. Plastic straining takes place with less crystallographic changes. In the region-3 with r > 20 μm, less KAM angles are detected. This region is still elastic.

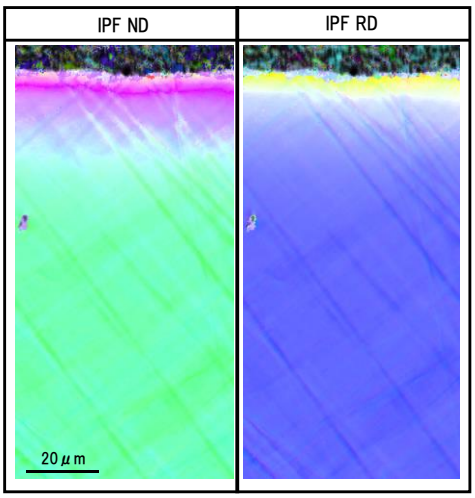

Figure 9 IPF distributions in ND and RD on the surface of single crystal at the vicinity of the pierced hole.

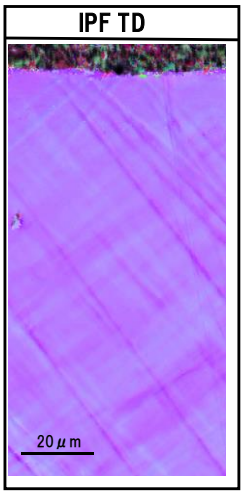

Figure 10 IPF distribution in TD on the surface of single crystal at the vicinity of the pierced hole.

In piercing under the narrow clearance between the nitrided punch and die, each Fe-6Si lattice in the single crystal at the vicinity of pierced hole is subjected to shear straining and hydrostatic pressure, respectively. The former straining accompanies with spin rotation to drive the crystallographic change in constituent lattices. The latter has nothing to do with this change. Hence, each lattice at the vicinity of

pierced hole is forced to rotate in the normal and rolling directions (ND and RD) but not to do in the tangential direction (TD). Let us demonstrate this prediction by EBSD analysis on the IPF distributions in the ND, RD and TD, respectively.

No crystallographic changes are seen in the region-3. The crystallographic orientation (101) vaguely starts from the border between region-2 and -3, and, significantly rotates from (101) to higher angled orientation between (001) and (111) both in ND and RD of region-1. This proves that the region-1 at the vicinity of pierced hole is an affected zone with large crystallographic orientation change by shearing. In the region-2, gradual crystallographic change in Fig. 9, implies that plastic straining takes place with a little spin rotation. No change in the region-3 also proves that no plastic straining nor spin rotation occurs by this piercing process.

Figure 10 depicts the IPF distribution in TD. No minor changes in crystallographic orientations are detected in the TD. This implies that no spin rotation occurs in the circumferential direction around the pierced hole.

The above IPF analyses by EBSD reveals that crystallographic reorientation from the original single-crystal state takes place in the radial and axial directions and that plastic straining advances in the symmetric condition around the pierced hole. This suggests that the plastic distortion induced by the piercing process consists of the shearing strains and spin rotation as well as the plastic straining by indentation of punch with hydrostatic pressure.

3.3. Material characterization on the affected zone

The affected zone width (W_A) by this piercing under the narrowed clearance of 3 μm or 1.5 % for the sheet thickness of 0.2 mm, is estimated to be 5 μm, where large crystallographic change takes place with piercing. This width is two times larger than the clearance. In case of fine piercing of AISI304 sheet, this width is thought to be the martensitic phase, transformed from the austenitic matrix [15]. With decreasing the clearance to zero, this width approaches to the minimum, where the spin rotation concentrates just at the vicinity of pierced hole.

3.4. Mechanical characterization on the plastic zone

The plastic zone width (W_P) by this piercing is estimated to be 20 μm or 10 % of sheet thickness. This width is four times larger than W_A. This mechanically affected zone corresponds to the work-hardened zone when piercing the AISI304 sheet [15]. Most of magnetic zones in this width is subjected to elastic recovery from the elasto-plastic state during piercing to the elastic state with residual strains after unloading.

4. Conclusion

Fine piercing process into single crystal Fe-6Si alloys is described by SEM and EBSD to define the material and mechanical affected zones. The material affected layer is characterized as a zone with large spin rotation by the crystallographic change in shearing. The mechanical affected layer is defined as an elasto-plastic zone to leave the residual strains. Qualitative analysis on these two zones provides a way to search for a piercing process with minimum iron loss.

Acknowledgements

The authors would like to express their gratitude to Mr. S. Kurozumi (Nano-Film Coat, LLC.) for his help in experiments. This study was financially supported in part by METI-project on the Supporting Industry Program at 2019.

References

[1] Y. Oda, T. Okubo, M. Takata, Recent development of non-oriented electrical steel in JFE steel. JFE Tech-Review 36 (2015) 6-11.

[2] T. Wakisaka, S. Arai, Y. Kurosaki, Electrical steel sheet for transaction motor of hybrid/electrical vehicles. Tech-Review, Shin-Nippon Steel 293 (2012) 116-120.

[3] S. R. Ning, J. Gao, Y. G. Wang, Review on applications of low loss amorphous metals in motors. Adv. Mater. Res. 129–131 (2010) 1366–1371.

[4] S. Doi, K. Fujiwara, Y. Takahashi, K. Okazaki, T. Aoki, Study of computational method of iron loss considering magnetic isotropic by processing residual stress. DENSO Tech-Review 23 (2018) 127-138.

[5] F. Ossart, R., Hug, O. Hubert, C. Buvat, R. Billardon, Effect of punching on electrical steels: Experimental and numerical coupled analysis. in Magnetics, IEEE Trans. 36 (5) (2000) 3137-3140.

[6] T. Shiratori, T. Aizawa, S. Nakano, T. Kato, Japan Patent (2019).

[7] E. Katsuta, T. Aizawa, H. Morita, K. Dohda, M. Anzai, Fine piercing of electromagnetic steel sheets by micro-punches under nearly zero clearance. Procedia Manufacturing 15 (2018) pp. 1459-1466.

[8] E. Katsuta, T. Aizawa, K. Dohda, S-I. Yoshihara, Fabrication of lower temperature plasma nitrided die and development of zero-clearance piercing of electromagnetic steel sheets. J. JSTP 60 (2019) pp. 70-74.

[9] T. AIzawa, T. Shiratori, T. Inohara, Short-pulse laser precise trimming of CVD-diamond coated punch for fine piecing. Proc. 2nd APSTP (Tokyo, Japan; August, 2019) 71-76.

[10] T. Aizawa, T. Shiratori, T. Yoshino, T. Inohara, Femtosecond laser trimming of CVD-diamond coated punch for fine embossing. Mater. Trans. 61 (2) (2020) 244-250.

[11] Z. Chen, Y. Yang, H. Jiao, Some applications of electron back scattering diffraction (EBSD) in materials research. InTech Open, (2012)

[12] Y. Yamamoto, Y. Hori, Solid Mechanics. Iwanami, Tokyo (1976) 179-190.

[13] L.A. Khan, V. Bhasin, J. Chattopadhyay, A.K. Ghosh, On the equivalence of slip-line fields and work principles for rigid-plastic body in plane strain. Int. J. Solids Struct. 45 (2008) 6416-6435.

[14] K. Nomura, K. Kubushiro, Y. Sakakibara, S. Takahashi, H. Yoshizawa, Effect of grain size on plastic strain analysis by EBSD for austenitic stainless steels with tensile strain at 650°C. J. JSMS 61 (2012) 371-376.

[15] T. Aizawa, T. Shiratori, T. Komatsu, Micro-/nano-structuring in stainless steels by metal forming and materials processing. Chap. 1 In: Crystallography. IntechOpen, UK, London (2020) 1-22.